

Reactions of *meso*-Hydroxyhemes with Carbon Monoxide and Reducing Agents in Search of the Elusive Species Responsible for the $g = 2.006$ Resonance of Carbon Monoxide-Treated Heme Oxygenase. Isolation of Diamagnetic Iron(II) Complexes of Octaethyl-*meso*-hydroxyporphyrin

Sankar Prasad Rath, Marilyn M. Olmstead, and Alan L. Balch*

Department of Chemistry, University of California, Davis, California 95616

Received March 30, 2004

To examine possible models for the $g = 2.006$ resonance seen when the hydroxylated heme–heme oxygenase complex in the Fe(III) state is treated with CO, the reactivities of CO and reducing agents with $(\text{py})_2\text{Fe}^{\text{III}}(\text{OEPO})$ and $\{\text{Fe}^{\text{III}}(\text{OEPO})\}_2$ (OEPO is the trianion of octaethyl-*meso*-hydroxyporphyrin) have been examined. A pyridine solution of $(\text{py})_2\text{Fe}^{\text{III}}(\text{OEPO})$ reacts in a matter of minutes with zinc amalgam (or with hydrazine) under an atmosphere of dioxygen-free dinitrogen to produce bright-red $(\text{py})_2\text{Fe}^{\text{II}}(\text{OEPOH}) \cdot 2\text{py} \cdot 0.33\text{H}_2\text{O}$, which has been isolated in crystalline form. The ^1H NMR spectrum of $(\text{py})_2\text{Fe}^{\text{II}}(\text{OEPOH})$ in a pyridine- d_5 solution is indicative of the presence of a diamagnetic compound, and no EPR resonance was observed for this compound. Treatment of a solution of $(\text{py})_2\text{Fe}^{\text{III}}(\text{OEPOH})$ in pyridine- d_5 with carbon monoxide produces spectral changes after a 30 s exposure that are indicative of the formation of diamagnetic $(\text{OC})(\text{py})\text{Fe}^{\text{II}}(\text{OEPOH})$. Treatment of a green pyridine solution of $(\text{py})_2\text{Fe}^{\text{III}}(\text{OEPO})$ with carbon monoxide reveals a slow color change to deep red over a 16 h period. Although a resonance at $g = 2.006$ was observed in the EPR spectrum of the sample during the reaction, the isolated product is EPR silent. The spectroscopic features of the final solution are identical to those of a solution formed by treating $(\text{py})_2\text{Fe}^{\text{II}}(\text{OEPOH})$ with carbon monoxide. Addition of hydrazine to solutions of $(\text{OC})(\text{py})\text{Fe}^{\text{II}}(\text{OEPOH})$ produces red, diamagnetic $(\text{OC})(\text{N}_2\text{H}_4)\text{Fe}^{\text{II}}(\text{OEPOH}) \cdot \text{py}$ in crystalline form. The X-ray crystal structures of $(\text{py})_2\text{Fe}^{\text{II}}(\text{OEPOH}) \cdot 2\text{py} \cdot 0.33\text{H}_2\text{O}$ and $(\text{OC})(\text{N}_2\text{H}_4)\text{Fe}^{\text{II}}(\text{OEPOH}) \cdot \text{py}$ have been determined. Solutions of diamagnetic $(\text{OC})(\text{N}_2\text{H}_4)\text{Fe}^{\text{II}}(\text{OEPOH}) \cdot \text{py}$ and $(\text{OC})(\text{py})\text{Fe}^{\text{II}}(\text{OEPOH})$ are extremely air sensitive and are immediately converted in a pyridine solution into paramagnetic $(\text{py})_2\text{Fe}^{\text{III}}(\text{OEPO})$ in the presence of dioxygen.

Introduction

This Article concerns model studies relevant to two unresolved issues in the operation of heme oxygenase. Heme oxygenase is a protein that binds unwanted heme and catalyzes its conversion into biliverdin, carbon monoxide, and ionic iron through oxidation that involves three dioxygen molecules.^{1–3} As seen in Scheme 1, several intermediates have been detected during the functioning of heme oxygenase.

The work reported here focuses on the step where the hydroxylated heme undergoes further oxidation to form verdoheme. The hydroxylated heme–heme oxygenase com-

plex contains a high-spin iron(III) site which produces EPR resonances at $g = 6$ and 2. Addition of carbon monoxide to the sample producing such a spectrum results in the formation a new, prominent free-radical-like resonance at $g = 2.008^4$ or 2.004.⁵ Similar observations have been made for the axial ligand mutants of mitochondrial cytochrome *b*₅, which have been hydroxylated with hydrogen peroxide and subsequently treated with carbon monoxide, where a resonance at $g = 2.006$ is observed.⁶ The species responsible for the $g = 2.008$, 2.006, or 2.004 resonance is considered to be the ferrous form of the hydroxylated heme in a radical form. In this complex, the Fe(II) state is believed to be stabilized by

* Author to whom correspondence should be addressed. E-mail: albalch@ucdavis.edu.

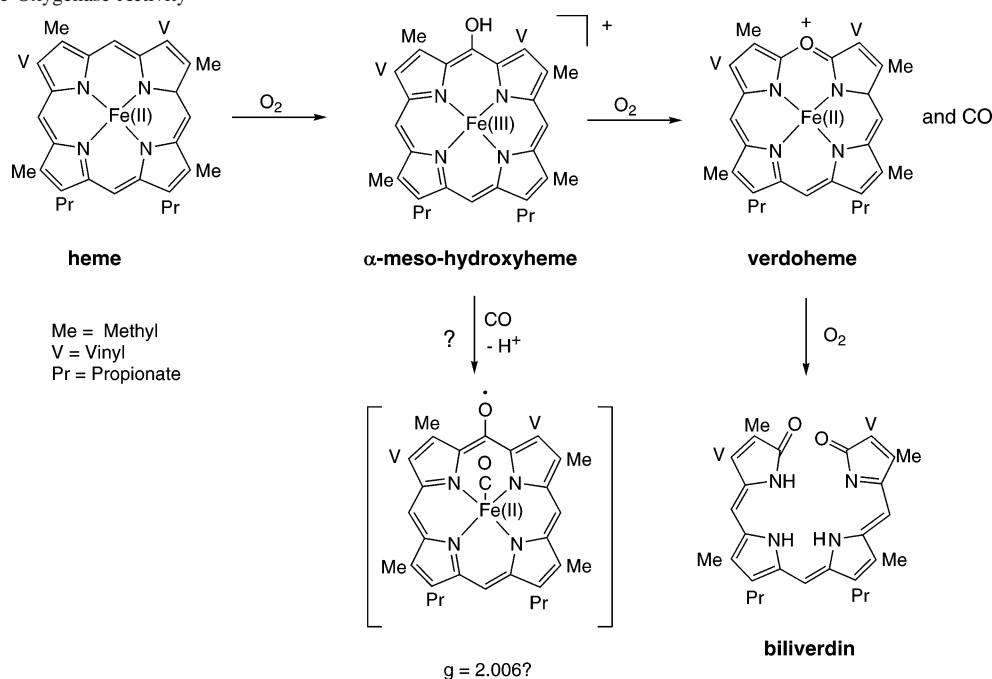
(1) Maines, M. D. *Heme Oxygenase: Clinical Applications and Functions*; CRC Press: Boca Raton, FL, 1992.
(2) Ortiz de Montellano, P. R. *Acc. Chem. Res.* **1998**, *31*, 543.
(3) Yoshida, T.; Migita, C. T. *J. Inorg. Biochem.* **2000**, *82*, 33.

(4) Liu, Y.; Moëne-Loccoz, P.; Loehr, T. M.; Ortiz de Montellano, P. R. *J. Biol. Chem.* **1997**, *272*, 6909.

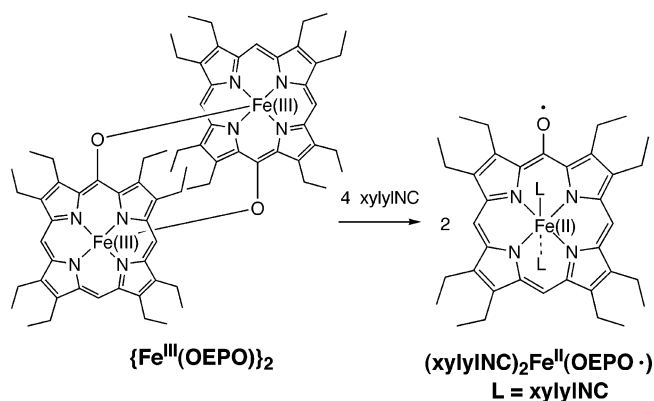
(5) Sakamoto, H.; Omata, Y.; Palmer, G.; Noguchi, M. *J. Biol. Chem.* **1999**, *274*, 18196.

(6) Avila, L.; Huang, H.; Damaso, C. O.; Lu, S.; Moëne-Loccoz, P.; Rivera, M. *J. Am. Chem. Soc.* **2003**, *125*, 4103.

Scheme 1. Heme Oxygenase Activity



Scheme 2



binding to carbon monoxide. However, no model complex involving carbon monoxide and an appropriately modified heme has yet been prepared. The closest available model for the form producing the $g = 2.008$, 2.006 , or 2.004 resonance is $(\text{xylylNC})_2\text{Fe}^{\text{II}}(\text{OEPO}\bullet)$,⁷ which was prepared from the previously characterized $\{\text{Fe}^{\text{III}}(\text{OEPO})_2\}$,^{8,9} complex, as shown in Scheme 2. The EPR spectrum of $(\text{xylylNC})_2\text{Fe}^{\text{II}}(\text{OEPO}\bullet)$ consists of a narrow line at $g = 2.008$, while its geometric structure is entirely consistent with a low-spin Fe(II) state.

The second unresolved issue involves the conversion of α -(*meso*-hydroxy)heme to verdoheme. This step is a chemically complex process that involves cleavage of two carbon-carbon bonds and the eventual release of carbon monoxide. The unresolved question is whether the five-coordinate, high-spin Fe(III) α -(*meso*-hydroxy)heme complex of heme oxygenase requires additional electrons before reacting with dioxygen to yield verdoheme or whether that intermediate reacts directly with dioxygen without an additional reducing agent. Thus, Ikeda-Saito and co-workers reported that the ferric hydroxyheme-heme oxygenase complex reacts directly with dioxygen and one electron to produce verdoheme.¹⁰ In contrast, Ortiz de Montellano and co-workers found that the Fe(III) α -(*meso*-hydroxy)heme-heme oxygenase complex reacts directly with dioxygen without the need for reducing equivalents to form the Fe(III) form of verdoheme.⁴ Palmer, Noguchi, and co-workers report that the Fe(III) α -(*meso*-hydroxy)heme complex of heme oxygenase is converted to verdoheme by reaction with dioxygen, again, without the need for an additional reducing agent.⁵ However, they found that verdoheme produced in this process is formed in the Fe(II) state. Migita and co-workers noted that the five-coordinate, high-spin Fe(III) α -(*meso*-hydroxy)heme-heme oxygenase complex can undergo oxidation with either dioxygen or [hexachloroiridium(IV)]²⁻ to yield a more highly oxidized form, with a modest shift in the Soret band from 405 to 401 nm.¹¹ Under these conditions, oxidation to form verdoheme is unproductive.

Here, we present results involving the addition of carbon monoxide to iron complexes of octaethyl-*meso*-hydroxyheme and examine the reactivity of iron(II) complexes of this ligand toward dioxygen and diiodine as oxidants.

Here, we present results involving the addition of carbon monoxide to iron complexes of octaethyl-*meso*-hydroxyheme and examine the reactivity of iron(II) complexes of this ligand toward dioxygen and diiodine as oxidants.

Results

Formation of Iron(II) Complexes, $(\text{py})_2\text{Fe}^{\text{II}}(\text{OEPOH})\cdot 2\text{py}\cdot 0.33\text{H}_2\text{O}$ and $(\text{OC})(\text{N}_2\text{H}_4)\text{Fe}^{\text{II}}(\text{OEPOH})\cdot \text{py}$. The reac-

(7) Rath, S. P.; Olmstead, M. M.; Balch, A. L. *J. Am. Chem. Soc.* **2004**, *126*, 6379.

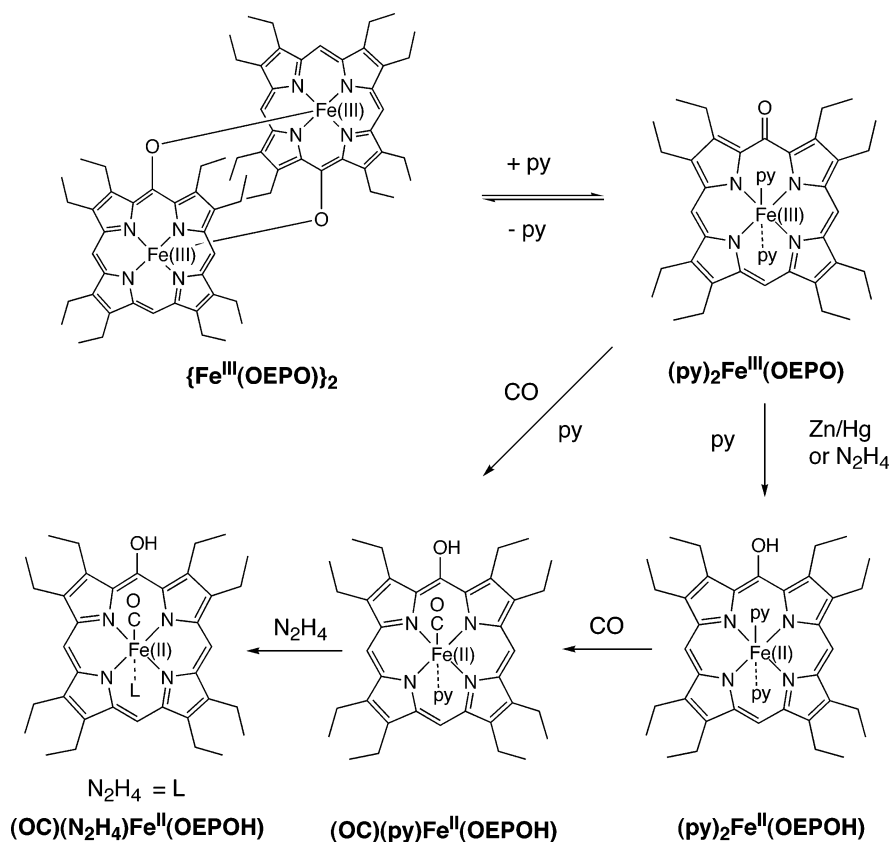
(8) Balch, A. L.; Latos-Grayski, L.; Noll, B. C.; Olmstead, M. M.; Zovinka, E. P. *Inorg. Chem.* **1992**, *31*, 2248.

(9) Lee, H. M.; Olmstead, M. M.; Gross, G. G.; Balch, A. L. *Cryst. Growth Des.* **2003**, *3*, 691.

(10) Matera, K. M.; Takahashi, S.; Fujii, H.; Zhou, H.; Ishikawa, K.; Yoshimura, T.; Rousseau, D. L.; Yoshida, T.; Ikeda-Saito, M. *J. Biol. Chem.* **1996**, *271*, 6618.

(11) Migita, C. T.; Fujii, H.; Matera, K. M.; Takahashi, S.; Zhou, H.; Yoshida, T. *Biochim. Biophys. Acta* **1999**, *1432*, 203.

Scheme 3



tions described here are summarized in Scheme 3. The complexes of the meso-hydroxylated porphyrins, $\{\text{Fe}^{\text{III}}(\text{OEPO})\}_2$ and $(\text{py})_2\text{Fe}^{\text{III}}(\text{OEPO})$, have been previously isolated and characterized by X-ray crystallography and NMR spectroscopy.^{9,14} Complexes $(\text{py})_2\text{Fe}^{\text{II}}(\text{OEPOH})$, $(\text{OC})(\text{py})\text{Fe}^{\text{II}}(\text{OEPOH})$, and $(\text{OC})(\text{N}_2\text{H}_4)\text{Fe}^{\text{II}}(\text{OEPOH})$ are new, and their preparations and characterizations are reported here.

Dissolution of a sample of $\{\text{Fe}^{\text{III}}(\text{OEPO})\}_2$ in a pyridine solution produces $(\text{py})_2\text{Fe}^{\text{III}}(\text{OEPO})$, which reacts in a matter of minutes with zinc amalgam under an atmosphere of dioxygen-free dinitrogen to produce a bright-red solution. Air-sensitive, red crystals of $(\text{py})_2\text{Fe}^{\text{II}}(\text{OEPOH}) \cdot 2\text{py} \cdot 0.33\text{H}_2\text{O}$ have been isolated from this solution. The UV-vis absorption spectra of this complex and of its precursor, $(\text{py})_2\text{Fe}^{\text{III}}(\text{OEPO})$, are shown in Figure 1. The spectrum of $(\text{py})_2\text{Fe}^{\text{II}}(\text{OEPOH})$ is similar to that of $(\text{py})_2\text{Fe}^{\text{II}}(\text{OEP})$ ¹² and is consistent with the presence of a low-spin ($S = 0$), six-coordinate iron(II) porphyrin. The ¹H NMR spectrum of $(\text{py})_2\text{Fe}^{\text{II}}(\text{OEPOH})$ in a pyridine-*d*₅ solution is shown in Figure 2A. The spectrum is indicative of the presence of a diamagnetic compound. The OH resonance is readily detected at 11.85 ppm, and there are two *meso*-H resonances in a 2:1 intensity ratio at 9.85 and 9.80 ppm. The methylene protons are observed at 4.36 and 3.95 ppm, while the methyl protons produce three resonances at 2.06, 1.02, and 1.90 ppm.

The reduction of $(\text{py})_2\text{Fe}^{\text{III}}(\text{OEPO})$ with zinc amalgam has also been monitored by EPR spectroscopy. As reduction

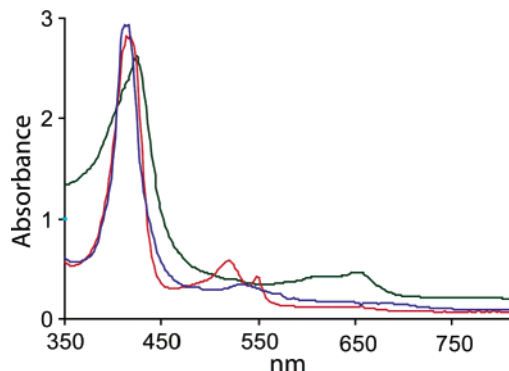


Figure 1. UV-vis spectra recorded under dioxygen-free conditions of $(\text{py})_2\text{Fe}^{\text{III}}(\text{OEPO})$ (green trace); $(\text{py})_2\text{Fe}^{\text{II}}(\text{OEPOH})$ (red trace); and $(\text{OC})(\text{py})\text{Fe}^{\text{II}}(\text{OEPOH})$ (blue trace).

occurs, the intensity of the signal at $g = 2.31$ and 1.78 decreases and a low-intensity free-radical signal at $g = 2.003$ develops. However, isolated samples of $(\text{py})_2\text{Fe}^{\text{II}}(\text{OEPOH}) \cdot 2\text{py} \cdot 0.33\text{H}_2\text{O}$ show no EPR spectra. Thus, the ¹H NMR and EPR results for isolated $(\text{py})_2\text{Fe}^{\text{II}}(\text{OEPOH}) \cdot 2\text{py} \cdot 0.33\text{H}_2\text{O}$ are consistent with the presence of a low-spin ($S = 0$) iron(II) complex. The origin of the $g = 2.003$ resonance in the EPR spectrum remains unidentified.

The reduction of $(\text{py})_2\text{Fe}^{\text{III}}(\text{OEPO})$ to form $(\text{py})_2\text{Fe}^{\text{II}}(\text{OEPOH})$ can also be accomplished by using hydrazine as the reducing agent. Samples of $(\text{py})_2\text{Fe}^{\text{II}}(\text{OEPOH})$ prepared by either route have identical spectroscopic properties.

The reactivities of $(\text{py})_2\text{Fe}^{\text{III}}(\text{OEPO})$ and $(\text{py})_2\text{Fe}^{\text{II}}(\text{OEPOH})$ toward carbon monoxide have been examined. Treatment of a solution of $(\text{py})_2\text{Fe}^{\text{II}}(\text{OEPOH})$ in pyridine-*d*₅ with carbon

(12) Bonnett, R.; Dimsdale, M. J. *J. Chem. Soc., Perkin Trans. 1* **1992**, 2540.

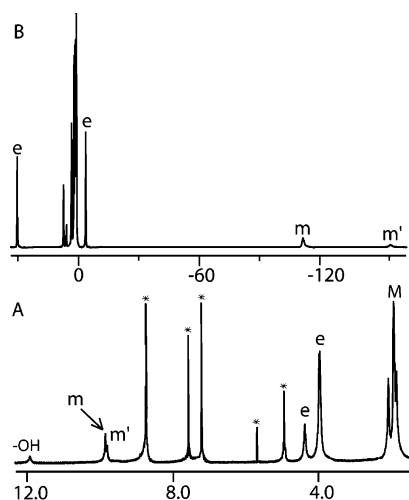


Figure 2. ^1H NMR spectrum of a pyridine- d_5 solution of $(\text{py})_2\text{Fe}^{\text{II}}(\text{OEPOH})$ (A) before and (B) after the addition of dioxygen.

monoxide produces spectral changes after a 30 s exposure that are indicative of the formation of diamagnetic $(\text{OC})\text{-(py)Fe}^{\text{II}}(\text{OEPOH})$. The UV-vis spectrum of the dark-red solution is shown in Figure 1 and is consistent with the formation of a carbonyl complex. The ^1H NMR spectrum of a solution of $(\text{OC})(\text{py})\text{Fe}^{\text{II}}(\text{OEPOH})$ shows an OH resonance at 12.6 ppm, meso resonances at 9.92 and 9.85 ppm, methylene resonances at 4.30 and 3.90 ppm, and methyl resonances at 2.06, 1.92, and 1.90 ppm at 298 K.

The reaction of carbon monoxide with $(\text{py})_2\text{Fe}^{\text{III}}(\text{OEPO})$ requires a longer period of time. Treatment of a green pyridine solution of $(\text{py})_2\text{Fe}^{\text{III}}(\text{OEPO})$ with carbon monoxide reveals a slow color change to deep red over a 16 h period. However, the spectroscopic features of the final solution are identical to those of a solution formed by treating $(\text{py})_2\text{Fe}^{\text{II}}(\text{OEPOH})$ with carbon monoxide. This reaction has also been followed by observing the EPR spectrum of the solution. During the reaction, the EPR spectrum of $(\text{py})_2\text{Fe}^{\text{III}}(\text{OEPO})$ slowly vanishes while a relatively weak signal develops at $g = 2.008$.

Solutions of $(\text{OC})(\text{py})\text{Fe}^{\text{II}}(\text{OEPOH})$ are extremely air sensitive. To isolate the carbon monoxide adduct in suitable crystalline form, it was necessary to add a reducing agent, hydrazine, to the sample to guard against oxidation. Under these conditions, hydrazine replaces pyridine as the axial ligand and it was possible to isolate the product, $(\text{OC})(\text{N}_2\text{H}_4)\text{-Fe}^{\text{II}}(\text{OEPOH})\cdot\text{py}$, in crystalline form. The infrared spectrum of the isolated crystals of $(\text{OC})(\text{N}_2\text{H}_4)\text{Fe}^{\text{II}}(\text{OEPOH})\cdot\text{py}$ shows a $\nu(\text{CO})$ at 1967 cm^{-1} . For comparison, $(\text{OC})(\text{py})\text{Fe}^{\text{II}}(\text{TPP})$ has a $\nu(\text{CO})$ at 1980 cm^{-1} .¹³ The ^1H NMR spectrum of $(\text{OC})\text{-(N}_2\text{H}_4)\text{Fe}^{\text{II}}(\text{OEPOH})\cdot\text{py}$ in toluene- d_7 (recorded at 203 K to minimize axial ligand exchange) shows the OH resonance at 12.15 ppm. There are two meso-H resonances in a 2:1 intensity ratio at 9.72 and 9.79 ppm. The methylene protons are observed at 3.85 and 3.77 ppm, while the methyl protons produce resonances at 2.17 and 1.81 ppm. The coordinated hydrazine protons produce two equally intense resonances at -3.50 and -3.97 ppm. The positions of these resonances

Table 1. Selected Bond Lengths (\AA) and Bond Angles (deg) for $(\text{py})_2\text{Fe}^{\text{II}}(\text{OEPOH})\cdot 2\text{py}\cdot 0.33\text{H}_2\text{O}$ (molecules 1 and 2) and $(\text{OC})(\text{N}_2\text{H}_4)\text{Fe}^{\text{II}}(\text{OEPOH})\cdot\text{py}$

	molecule 1	molecule 2	$(\text{OC})(\text{N}_2\text{H}_4)\text{Fe}^{\text{II}}(\text{OEPOH})\cdot\text{py}$
Bond Lengths			
Fe–N1	1.997(4)	2.002(4)	2.013(3)
Fe–N2	1.992(4)	1.991(4)	2.015(3)
Fe–N3	2.017(4)	2.004(4)	2.012(3)
Fe–N4			2.006(3)
Fe–N5			2.069(3)
Fe–C37			1.767(4)
C37–O2			1.153(4)
C1–O5,	1.395(16)	1.403(18)	1.429(6)
C1–O1			
C10–O2,	1.292(13)	1.377(11)	1.454(12)
C5–O1B			
Bond Angles			
N1–Fe–N2	89.19(16)	89.56(16)	88.84(12)
N1–Fe–N3	88.66(16)	89.20(16)	174.73(13)
N1–Fe–N4			91.09(13)
N1–Fe–N5			88.64(12)
N1–Fe–C37			92.87(15)
N2–Fe–N3	91.03(16)	91.42(17)	90.67(12)
N2–Fe–N4			176.77(13)
N2–Fe–C37			91.83(15)
N3–Fe–N4			89.11(13)
N3–Fe–N5			86.10(12)
N3–Fe–C37			92.38(15)
N4–Fe–N5			88.68(13)
N4–Fe–C37			91.40(16)
N5–Fe–C37			178.48(16)
Fe–C37–O2			179.1(4)
Fe–N5–N6			120.9(3)

are caused by the positioning of the axial ligand protons in a region where the ring current of the porphyrin ligand produces upfield shifts. Thus, the ^1H NMR spectrum is indicative of the formation of a diamagnetic iron(II) complex. There is no EPR spectrum detected from an isolated crystalline sample of $(\text{OC})(\text{N}_2\text{H}_4)\text{Fe}^{\text{II}}(\text{OEPOH})\cdot\text{py}$.

Single-Crystal X-ray Diffraction of $(\text{py})_2\text{Fe}^{\text{II}}(\text{OEPOH})\cdot 2\text{py}\cdot 0.33\text{H}_2\text{O}$. The complex crystallizes in the triclinic space group $P\bar{1}$. There are two half-molecules of the complex in the asymmetric unit. The iron atom in each molecule is located at a center of symmetry. Selected interatomic distances and angles are given in Table 1. Crystal data are given in Table 2. Figure 3 shows the structure of one of the complexes (molecule 2). The iron is, as expected, six-coordinate. The neighboring water molecule with a fractional occupancy of 0.33 is hydrogen bonded to the meso-OH group. The structure of molecule 1 is similar to that of molecule 2, as the data in Table 1 show. However, in molecule 1, there is no hydrogen bonding from the meso-OH group to a water molecule.

In both molecules, the oxygen atom is disordered equally over the four meso positions. This type of disorder is common in derivatives of the octaethylporphyrin that have a small substituent attached to one meso-carbon atom. For example, the position of the meso-oxygen in $(\text{py})_2\text{Fe}^{\text{III}}(\text{OEPO})$ is disordered.¹⁴ Related cases of disorder are seen in $\text{ClFe}^{\text{III}}(\text{meso-NC-OEP})$,¹⁵ $\text{Zn}^{\text{II}}(\text{OEPO})$,¹⁶ and $(1\text{-MeIm})_2\text{-}$

(13) Peng, S.-M.; Ibers, J. A. *J. Am. Chem. Soc.* **1976**, *98*, 8032.

(14) Balch, A. L.; Koerner, R.; Latos-Grażyński, L.; Noll, B. C. *J. Am. Chem. Soc.* **1996**, *118*, 2760.

(15) Kalish, H.; Camp, J. E.; Stępień, M.; Latos-Grażyński, L.; Olmstead, M. M.; Balch, A. L. *Inorg. Chem.* **2002**, *41*, 989.

Table 2. Crystal Data and Data Collection Parameters

	(py) ₂ Fe ^{II} (OEPOH)·2py·0.33H ₂ O	(OC)(N ₂ H ₄)Fe ^{II} (OEPOH)·py
formula	C ₅₆ H _{62.67} FeN ₈ O _{1.33}	C ₄₂ H ₅₃ FeN ₇ O ₂
formula weight	925.02	743.76
color and habit	red plate	red plate
crystal system	triclinic	triclinic
<i>T</i> (K)	90(2)	91(2)
space group	<i>P</i> $\bar{1}$	<i>P</i> $\bar{1}$
<i>a</i> (Å)	13.2142(16)	10.6806(15)
<i>b</i> (Å)	15.1619(18)	13.4729(19)
<i>c</i> (Å)	15.3635(19)	13.869(2)
α (deg)	106.478(2)	78.066(3)
β (deg)	99.010(2)	76.444(3)
γ (deg)	110.242(2)	86.994(3)
<i>V</i> (Å ³)	2656.1(6)	1898.1(5)
radiation Mo K α , λ (Å)	0.71073	0.71073
<i>Z</i>	2	2
<i>d</i> _{calcd} (g cm ⁻³)	1.157	1.301
μ (mm ⁻¹)	0.329	0.443
range of transm factors	0.88–0.98	0.84–1.00
no. of unique data	9710	8631
no. of restraints	0	6
no. of params refined	581	498
R1 ^a	0.078	0.067
wR2 ^b	0.235	0.201

^a For data with $I > 2\sigma(I)$. $R1 = \sum||F_o| - |F_c||/\sum|F_o|$. ^b For all data. $wR2 = \sqrt{\sum[w(F_o^2 - F_c^2)^2]/\sum[w(F_o^2)^2]}$.

Fe^{III}(OEPO).⁷ The presence of external hydrogen bonding to the *meso*-OH group can produce situations in which the position of this hydroxyl group is fixed, as is the case in (py)Zn^{II}(OEPOH···py).¹⁶ However, the hydrogen bonding of molecule 2 to the adjacent water molecule is not sufficient in the present case to produce ordering of the location of the *meso*-OH groups in this crystal.

Since the complexes are both centrosymmetric, the planes of the two axial ligands are rigorously parallel to one another. As part B of Figure 3 shows, these ligands are staggered with respect to the in-plane Fe–N bonds, with angles between the plane of the axial ligands and the adjacent Fe–N bond of 40.4° in molecule 1 and 43.3° in molecule 2. This orientation of the axial ligand planes is consistent with prior observations of the locations of axial heterocyclic amines in low-spin, iron(II) porphyrins.^{17,18} Since the *meso*-OH groups are disordered in four sites, the positioning of the planes of the axial ligands does not appear to be correlated with the location of the *meso*-OH group. The orientation of the axial ligands in (py)₂Fe^{II}(OEPOH)·2py·0.33H₂O can also be compared with the ligand orientation in (py)₂Fe^{III}(OEPO). In the latter case, the ligands are required by the crystallographic center of symmetry to be parallel, but they eclipse the Fe–N bonds so that the angle between the plane of the pyridine ligand and the adjacent Fe–N bond is only 13.3°.

The O1–C5 distance in molecule 1 is 1.395(16) Å, a distance that is indicative of a C–O single bond. However, in molecule 2 the C2–O10 distance is 1.292(13) Å.

The Fe–N1 and Fe–N2 distances, which are the in-plane distances to the porphyrin nitrogen atoms, are 1.997(4) and

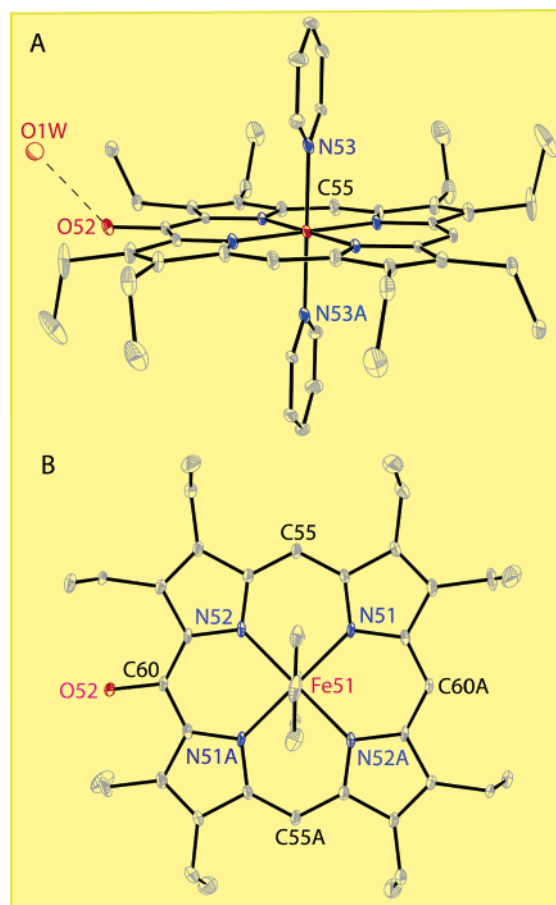


Figure 3. (A) Perspective view of molecule 2 of (py)₂Fe^{II}(OEPOH)·2py·0.33H₂O showing 30% thermal contours. Only one of the four sites for the *meso*-oxygen atom is shown. This site has a fractional occupancy of 0.29. The site of the water molecule with 0.33 occupancy is also shown. The O52···O1W bond distance is 2.71(2) Å. (B) View of the same molecule looking down on the porphyrin plane and showing the relative orientations of the two axial ligands.

1.992(4) Å, respectively. The axial Fe–N3 distance is slightly longer at 2.017(4) Å. These distances are similar to those observed for other low-spin iron(II) porphyrins.^{16,17}

The porphyrin macrocycles in both molecules of (py)₂Fe^{II}(OEPOH)·2py·0.33H₂O are nearly planar. Figure 4 shows the displacements of the porphyrin core atoms from the plane of the macrocycle. The largest out-of-plane displacement of any of the core atoms is only 0.036 Å for C8 in molecule 1 and 0.065 Å for C58 in molecule 2.

Single-Crystal X-ray Diffraction of (OC)(N₂H₄)Fe^{II}(OEPOH)·py. The complex crystallizes with one molecule in the asymmetric unit with no crystallographically imposed symmetry. Figure 5 shows a drawing of the six-coordinate iron complex and the adjacent pyridine ligand to which it is hydrogen bonded through the *meso*-OH group. Bond distances and angles are given in Table 1.

The structure of (OC)(N₂H₄)Fe^{II}(OEPOH)·py is similar to that of the porphyrin complex (OC)(py)Fe^{II}(TPP) reported earlier.¹³ It is also related to the macrocyclic complexes, (OC)(py)Fe^{II}(C₂₂H₂₂N₄) and (OC)(N₂H₄)Fe^{II}(C₂₂H₂₂N₄), whose structures are shown in Scheme 4.¹⁹

The in-plane Fe–N bond distances to the macrocycle fall in a narrow range, 2.006(3)–2.015(3) Å, and are similar in

(16) Balch, A. L.; Noll, B. C.; Zovinka, E. P. *J. Am. Chem. Soc.* **1992**, *114*, 3380.

(17) Safo, M. K.; Nasset, M. J. M.; Walker, F. A.; Debrunner, P. G.; Scheidt, W. R. *J. Am. Chem. Soc.* **1997**, *119*, 9438.

(18) Safo, M. K.; Scheidt, W. R.; Gupta, G. P. *Inorg. Chem.* **1990**, *29*, 626.

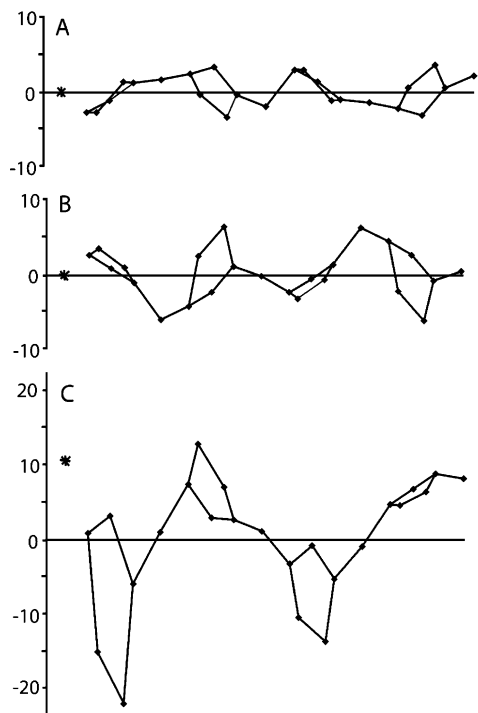


Figure 4. Diagrams showing the out-of-plane displacements of the porphyrin core atoms from the mean plane of the porphyrin for molecules 1 (A) and 2 (B) of $(\text{py})_2\text{Fe}^{\text{II}}(\text{OEPOH})\cdot 2\text{py}\cdot 0.33\text{H}_2\text{O}$ and for $(\text{OC})(\text{N}_2\text{H}_4)\text{Fe}^{\text{II}}(\text{OEPOH})\cdot \text{py}$ (C) in units of 0.01 Å. The position of the iron atoms is shown by an asterisk. Due to the disorder, the position of the *meso*-OH group is not denoted.

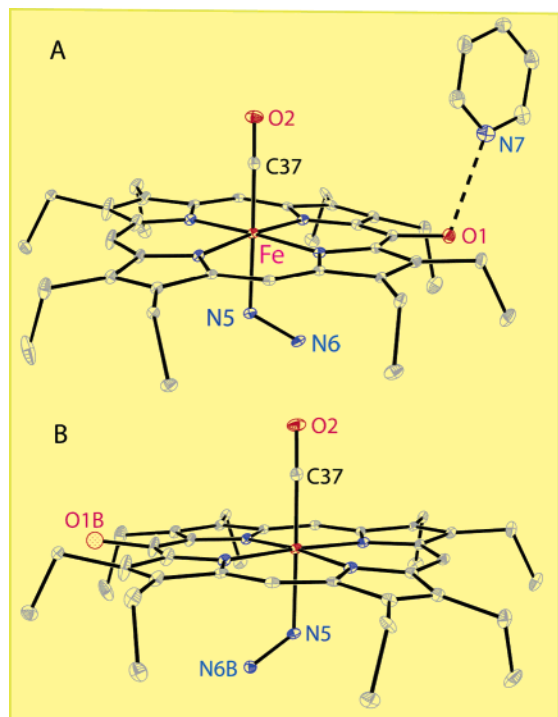
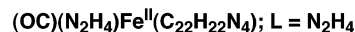
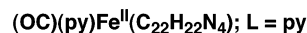
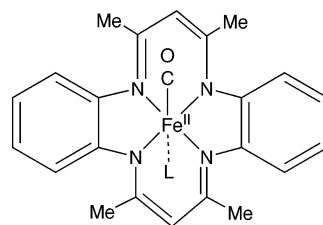


Figure 5. Perspective view of $(\text{OC})(\text{N}_2\text{H}_4)\text{Fe}^{\text{II}}(\text{OEPOH})\cdot \text{py}$ showing 30% thermal contours. The view in A shows the major form with partially occupied positions for O1 (0.72 occupancy) and N6 (0.70 occupancy) and the hydrogen bonding between O1 and the adjacent pyridine with the $\text{N7}\cdots\text{O1}$ bond distance of 2.791(6) Å. The view in B shows the minor form with the alternate locations of O1B (0.28 occupancy) and N6B (0.30 occupancy).

length to those of the two molecules of $(\text{py})_2\text{Fe}^{\text{II}}(\text{OEPOH})\cdot 2\text{py}\cdot 0.33\text{H}_2\text{O}$ and to other Fe(II) porphyrins.^{17,18} The Fe—

Scheme 4



C37 bond length, 1.767(4) Å, is similar to the corresponding distances in $(\text{OC})(\text{py})\text{Fe}^{\text{II}}(\text{TPP})$ [1.77(2) Å],¹³ $(\text{OC})(\text{py})\text{Fe}^{\text{II}}(\text{C}_{22}\text{H}_{22}\text{N}_4)$ [1.730(3) Å],¹⁹ and $(\text{OC})(\text{N}_2\text{H}_4)\text{Fe}^{\text{II}}(\text{C}_{22}\text{H}_{22}\text{N}_4)$ [1.751(5) Å].¹⁹ The Fe—C37—O2 bond angle [179.2(3)°] is nearly linear and similar to those in $(\text{OC})(\text{py})\text{Fe}^{\text{II}}(\text{C}_{22}\text{H}_{22}\text{N}_4)$ [178.2(3)°]¹⁹ and $(\text{OC})(\text{N}_2\text{H}_4)\text{Fe}^{\text{II}}(\text{C}_{22}\text{H}_{22}\text{N}_4)$ [177.6(5)°].¹⁹ The Fe—N5 distance is 2.069(3) Å and is longer than the in-plane Fe—N distances. For comparison, the Fe—N distance in $(\text{OC})(\text{N}_2\text{H}_4)\text{Fe}^{\text{II}}(\text{C}_{22}\text{H}_{22}\text{N}_4)$ is 2.122(5) Å.¹⁹ This lengthening of the axial Fe—N distance can be attributed to the strong trans effect of the coordinated carbon monoxide. The Fe—N5—N6 angle is 120.9(3)°, which is similar to the corresponding angle [121.3(3)°] in $(\text{OC})(\text{N}_2\text{H}_4)\text{Fe}^{\text{II}}(\text{C}_{22}\text{H}_{22}\text{N}_4)$.¹⁹

As seen in Figure 4, the porphyrin is slightly distorted from planarity. The iron ion is displaced by 0.106 Å from the plane of the porphyrin toward the carbon monoxide ligand.

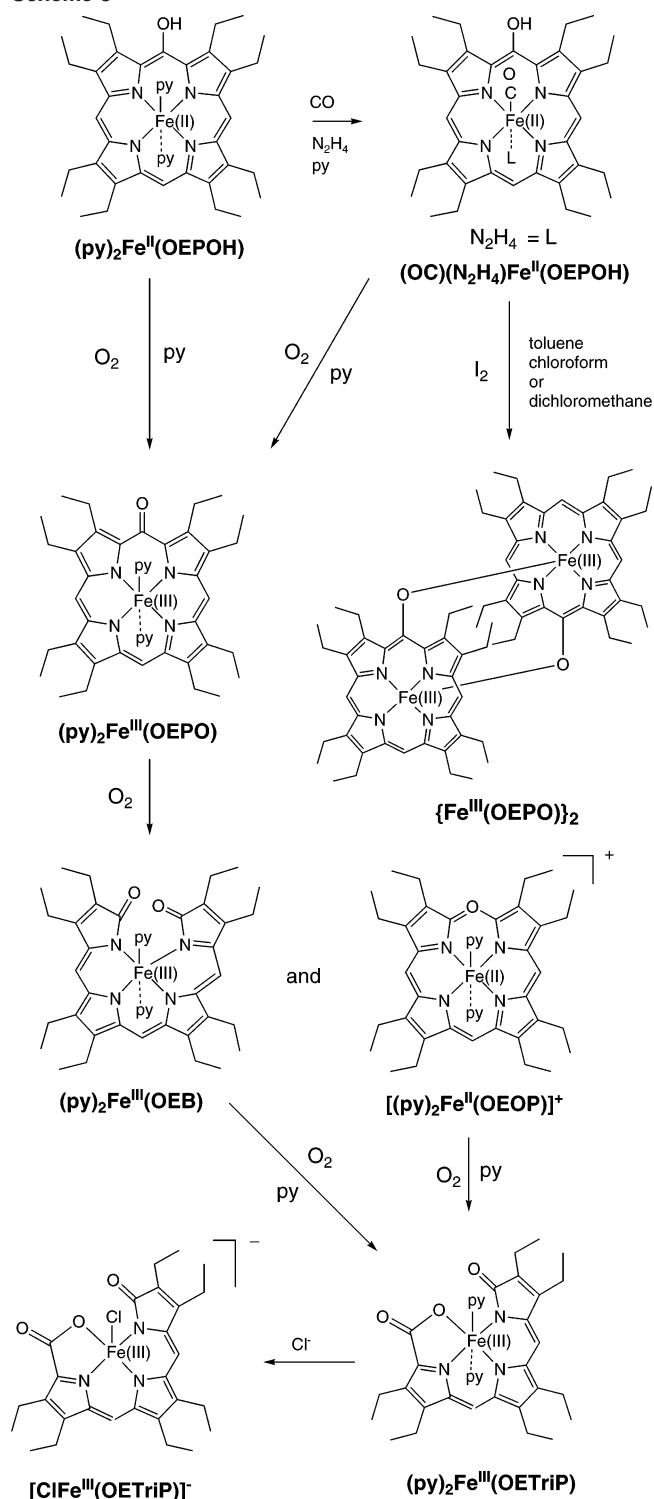
Although hydrogen bonding to the nearby pyridine ligand produces substantial ordering of the location of the *meso*-OH group, there is a minor OH site with a 0.28 fractional occupancy, which is shown in part B of Figure 5. There is also disorder in the position of the hydrazine ligand. The minor site with a 0.30 fractional occupancy is also shown in part B of Figure 5. Although the minor sites of the *meso*-OH group and the hydrazine nitrogen have similar occupancies, there may be no actual correlation between the occupancy of these two sites, as implied by Figure 5. The two *meso*-C—O bond distances are consistent with a single bond between carbon and oxygen. In $(\text{py})_2\text{Fe}^{\text{III}}(\text{OEPO})$, where there is no hydrogen attached to the *meso*-O, the C—O bond is shorter [1.289(4) Å] at the major site and the minor site [1.340(13) Å].¹⁴

Oxidation Reactions. Solutions of $(\text{py})_2\text{Fe}^{\text{II}}(\text{OEPOH})$ and $(\text{CO})(\text{N}_2\text{H}_4)\text{Fe}^{\text{II}}(\text{OEPOH})$ are extremely sensitive to oxidation. The reactions that occur upon addition of dioxygen or diiodine are summarized in Scheme 5.

When dioxygen is added to a solution of $(\text{py})_2\text{Fe}^{\text{II}}(\text{OEPOH})$, the ¹H NMR spectrum immediately changes, as shown in Figure 2. The resonances of diamagnetic $(\text{py})_2\text{Fe}^{\text{II}}(\text{OEPOH})$ vanish and are replaced by those of paramagnetic $(\text{py})_2\text{Fe}^{\text{III}}(\text{OEPO})$. The ¹H NMR spectrum of $(\text{py})_2\text{Fe}^{\text{III}}(\text{OEPO})$ has been reported and thoroughly analyzed previ-

(19) Goedken, V. L.; Peng, S.-M.; Molin-Norris, J.; Park, Y. *J. Am. Chem. Soc.* **1976**, *98*, 8391.

Scheme 5



ously.^{20–22} The conversion of $(py)_2Fe^{II}(OEPOH)$ into $(py)_2Fe^{III}(OEPO)$ can also be accomplished by the addition of diiodine. Similar 1H NMR spectral changes accompany the diiodine oxidation. Solutions of $(py)_2Fe^{III}(OEPO)$ in pyridine are also sensitive to prolonged exposure to dioxygen, as shown previously.²³ The next step in the reaction is the slower formation of a mixture of the diamagnetic verdoheme $[Fe^{II}(OEOP)]^+$ and iron biliverdin complex $(py)_2Fe^{III}(OEB)$,

(20) Morishima, I.; Fujii, H.; Shiro, Y. *J. Am. Chem. Soc.* **1986**, *108*, 3858.

which are also air sensitive, and these are subsequently converted into the tripyrrole complex, $(py)_2Fe(\text{tripyrrole})$, as reported earlier.²³

Solutions of $(OC)(N_2H_4)Fe^{II}(OEPOH) \cdot py$ in pyridine are also sensitive to dioxygen. Exposure to dioxygen produces $(py)_2Fe^{III}(OEPO)$, as shown by changes in the 1H NMR spectrum of the sample. This oxidation has also been monitored by EPR. During the reaction, no free-radical-like signal appeared in the vicinity of $g = 2.006$. In contrast, Masuoka and Itano did detect an EPR resonance at $g = 2.008$ during the exposure of a sample of $(py)_2Fe^{III}(OEPO)$ to dioxygen.²⁴ However, the intensity of that resonance was low and estimated to represent about one-hundredth of that of the $(py)_2Fe^{III}(OEPO)$ present. Addition of diiodine to a solution of $(OC)(N_2H_4)Fe^{II}(OEPOH) \cdot py$ in toluene, benzene, chloroform, or dichloromethane takes a different course of reaction. This reaction has been monitored by 1H NMR spectroscopy and cleanly produces the dimer, $\{Fe^{III}(OEPO)\}_2$. Again, when the reaction was monitored by EPR spectroscopy, no resonance near $g = 2.006$ was detected.

Discussion

This work has resulted in the isolation of two low-spin iron(II) complexes of meso-hydroxylated octaethylporphyrin. Both are extremely sensitive to dioxygen and are converted to the sequence of the heme cleavage products shown in Scheme 5. For these oxidations, which involve the simple heme itself in a strongly coordinating environment (pyridine solution), there is no need for additional reducing equivalents. The iron(II) hemes, $(py)_2Fe^{II}(OEPOH)$ and $(OC)(N_2H_4)Fe^{II}(OEPOH) \cdot py$, react directly with dioxygen to begin the process of heme ring opening. While this new information does not resolve the controversy surrounding the need of reducing equivalents after the initial stage of heme hydroxylation in heme oxygenase, it does establish the fundamental fact that low-spin iron(II) complexes of the hydroxylated heme are intrinsically reactive toward dioxygen. The initial product of that oxidation in pyridine solution is $(py)_2Fe^{III}(OEPO)$, and this complex readily undergoes additional oxidative cleavage, as shown in Scheme 5.

The species responsible for the EPR resonance at $g = 2.006$ seen when heme oxygenase and related proteins are treated with carbon monoxide has not been identified in the experiments reported here. The two new complexes isolated here, $(py)_2Fe^{II}(OEPOH) \cdot 2py \cdot 0.33H_2O$ and $(OC)(N_2H_4)Fe^{II}(OEPOH) \cdot py$, are normal diamagnetic iron(II) complexes, which do not show any EPR resonance. A relatively weak signal at $g = 2.008$ does appear when carbon monoxide reacts with $(py)_2Fe^{III}(OEPO)$ as noted above, but the species responsible for this resonance appears to be a minor component that we have not been able to isolate. Additionally, the reduction of $(py)_2Fe^{III}(OEPO)$ with zinc amalgam

(21) Morishima, I.; Shiro, Y.; Hiroshi, F. *Inorg. Chem.* **1995**, *34*, 1528.

(22) Kalish, H.; Camp, J. E.; Stepien, M.; Latos-Grażyński, L.; Balch, A. L. *J. Am. Chem. Soc.* **2001**, *123*, 11719.

(23) Rath, S. P.; Olmstead, M. M.; Latos-Grażyński, L.; Balch, A. L. *J. Am. Chem. Soc.* **2003**, *125*, 12678.

(24) Masuoka, N.; Itano, H. A. *Biochemistry* **1987**, *26*, 3672.

in the absence of carbon monoxide produces a weak free-radical signal at $g = 2.003$; the species responsible for this resonance has not been isolated, and it also appears to be a minor component in the reaction mixture. It also should be noted that radical-like EPR resonances have been observed at $g = 2.004$ and 2.0012 during the oxygenation of α -oxyprotoheme IX that is incorporated into apomyoglobin.²⁵ No carbon monoxide was added to the sample during that study. Finally, a resonance at $g = 2.008$ was detected during the treatment of $(\text{py})_2\text{Fe}^{\text{III}}(\text{OEPO})$ with dioxygen,²⁴ but we were unable to reproduce this observation. Thus, the complex or complexes responsible for the free-radical-like EPR resonances in the $g = 2.008$ – 2.001 range that are produced during reactions of meso-oxygenated hemes remain elusive entities. We have shown that the well-characterized complex $(\text{xylylNC})_2\text{Fe}^{\text{II}}(\text{OEPO}\bullet)$, which has been isolated in pure crystalline form and characterized by X-ray crystallography, does produce an EPR resonance at $g = 2.008$. This complex represents one case in which the ligand radical form of the macrocycle is stabilized by having axial ligands present that favor the Fe(II) oxidation state. Carbon monoxide is similar to isocyanide in many respects. However, hemes with two axial carbon monoxide ligands, which would be needed to produce an analogue of $(\text{xylylNC})_2\text{Fe}^{\text{II}}(\text{OEPO}\bullet)$, are not particularly stable.²⁶ It is possible that the species responsible for the free-radical-like EPR resonances in the $g = 2.006$ region, produced by treating the hydroxylated heme–heme oxygenase complex with carbon monoxide, involve carbon monoxide in conjunction with another axial ligand that is not present in the model systems utilized in the studies reported here. Alternately, that resonance may arise from a non-heme site. Further information quantifying the intensity of these EPR resonances in the $g = 2.006$ region found for the samples of heme oxygenase would be valuable for evaluating their significance.

The Fe–C37–O2 bond angle in $(\text{OC})(\text{N}_2\text{H}_4)\text{Fe}^{\text{II}}(\text{OEPOH})\text{py}$ [$179.2(3)^\circ$] is nearly linear, as are other isolated model complexes containing low-spin Fe^{II}–CO units.^{13,19} For comparison, the crystal structures of heme oxygenases with carbon monoxide bound to normal heme (not hydroxylated heme as studied here) have revealed that the Fe–C–O unit is bent to 170° for heme oxygenase from *Neisseriae meningitidis*, with only 0.050 site occupancy for CO,²⁷ and 158° for rat heme oxygenase-1.²⁸ Such bending of the Fe–C–O unit is also seen in the carbon monoxide-bound heme in myoglobin,²⁹ which has a heme binding site that is similar to that in heme oxygenase and in heme model complexes where steric constraints force the Fe–C–O unit to bend.^{30–32} Thus, the observed bending of the Fe–C–O unit in the heme oxygenase structures can be attributed to the nature of the

heme-binding pocket and the steric constraints that the protein imposes.

Experimental Section

Materials. Iron(III) octaethylporphyrin chloride was purchased from Mid Century. Samples of $\{\text{Fe}^{\text{III}}(\text{OEPO})\}_2$ were prepared by an established route.³³ Pyridine-*d*₅ was used after further distillation with potassium hydroxide under a dinitrogen atmosphere. All of the solvents used were carefully degassed by five freeze/pump/thaw cycles prior to use.

Preparation of $(\text{py})_2\text{Fe}^{\text{II}}(\text{OEPOH})\cdot 2\text{py}\cdot 0.33\text{H}_2\text{O}$. Under an atmosphere of purified dinitrogen in a glovebox, 50 mg (0.043 mmol) of $\{\text{Fe}^{\text{III}}(\text{OEPO})\}_2$ was dissolved in 5 mL of dry pyridine and 600 μL (10.8 mmol) of degassed hydrazine (95% in H₂O) was added. The solution color immediately turned red. After *n*-hexane was carefully layered over the sample solution, red crystals, suitable for X-ray crystallography, grew in 7–8 days. Yield: 40.1 mg (50%).

Preparation of $(\text{OC})(\text{N}_2\text{H}_4)\text{Fe}^{\text{II}}(\text{OEPOH})\cdot \text{py}$. Under an atmosphere of purified dinitrogen in a glovebox, 50 mg (0.043 mmol) of $\{\text{Fe}^{\text{III}}(\text{OEPO})\}_2$ was dissolved in 5 mL of dry pyridine and 500 μL (9.0 mmol) of degassed hydrazine (95% in water) was added. The solution color immediately turned red. Carbon monoxide was passed through the solution for 30 s. Carbon monoxide-saturated diethyl ether was layered over the sample. After 7–8 days, the black crystals suitable for X-ray crystallographic work grew. These were collected by filtration and dried. Yield: 33 mg (52%).

Preparation of $(\text{OC})(\text{py})\text{Fe}^{\text{II}}(\text{OEPOH})$. Method 1. A 2 mmol, pink-red solution of $\text{Fe}^{\text{II}}(\text{OEPOH})(\text{py})_2$ in pyridine-*d*₅ was placed in the NMR tube in a dry dinitrogen atmosphere and the tube sealed with a rubber septum. Carbon monoxide was passed through the solution for 30 s at 22 °C. The sample was shaken for another 30 s. A dark-red solution was obtained, which was used for ¹H NMR spectroscopic observation.

Method 2. A 50 mg (0.043 mmol) sample of $\{\text{Fe}^{\text{III}}(\text{OEPO})\}_2$ was dissolved in 20 mL of degassed pyridine under a dinitrogen atmosphere and stirred in a stream of dry CO that was passed through the solution for 5 min. The sample was sealed and kept in a dinitrogen-filled glovebox for 16 h. During this time, the green solution turned deep red. The sample was evaporated to dryness in vacuum. The brown solid product was isolated and used for spectroscopic investigation.

X-ray Data Collection. Crystals of the two complexes were obtained directly from the preparations as described above. The crystals were cooled in dry ice to minimize solvent loss, immediately coated with a light hydrocarbon oil, and mounted in the 90 K dinitrogen stream of a Bruker SMART 1000 diffractometer equipped with a CRYO Industries low-temperature apparatus. Intensity data were collected using graphite monochromated Mo K α radiation. Crystal data are given in Table 2.

Solution and Structure Refinement. Scattering factors and corrections for anomalous dispersion were taken from a standard source.³⁴ An absorption correction was applied.³⁵ The solution of the structure was obtained by direct methods using SHELXS-97

(25) Sano, S.; Sano, T.; Morishima, I.; Shiro, Y.; Maeda, Y. *Proc. Natl. Acad. Sci. U.S.A.* **1986**, *83*, 531.

(26) Wayland, B. B.; Mehne, L. F.; Swartz, J. J. *Am. Chem. Soc.* **1978**, *100*, 2379.

(27) Friedman, J.; Lad, L.; Deshmukh, R.; Li, H.; Wilks, A.; Poulos, T. L. *J. Biol. Chem.* **2003**, *278*, 34654.

(28) Sugishima, M.; Sakamoto, H.; Noguchi, M.; Fukuyama, K. *Biochemistry* **2003**, *42*, 9898.

(29) Vojtěchovský, J.; Chu, J.; Berendzen, J.; Sweet, R. M.; Schlichting, I. *Biophys. J.* **1999**, *77*, 2153.

(30) Kim, K.; Fetting, J.; Sessler, J.; Cyr, M.; Hugdahl, J.; Collman, J. P.; Ibers, J. A. *J. Am. Chem. Soc.* **1989**, *111*, 403.

(31) Kim, K.; Ibers, J. A. *J. Am. Chem. Soc.* **1991**, *113*, 6077.

(32) Slebodnick, C.; Duval, M. L.; Ibers, J. A. *Inorg. Chem.* **1996**, *35*, 3607.

(33) Balch, A. L.; Koerner, R.; Latos-Grażyński, L.; Lewis, J. E.; St. Claire, T. N.; Zovinka, E. P. *Inorg. Chem.* **1997**, *36*, 3892.

and subsequent cycles of least-squares refinement on F^2 with SHELXL-97.

Instrumentation. ^1H NMR spectra were recorded on a Bruker Avance 500 FT spectrometer (^1H frequency is 500.1100 MHz). The spectra were recorded over a 100 kHz bandwidth with 32K data points and a $5\ \mu\text{s}$ 90° pulse. For a typical spectrum between 500 and 1000, transients were accumulated with a 250 ms repetition time. The residual ^1H resonances of the solvent were used as secondary chemical shift references. The X-band EPR spectra were recorded on a Bruker ECS-106 instrument, equipped with an Oxford

Instruments variable-temperature liquid-helium cryostat. The microwave frequency was measured by using a calibrated cavity resonator, and the magnetic field intensity was checked using solid DPPH as a standard.

Acknowledgment. We thank the NIH (Grant GM-26226, A.L.B.) and the NSF (Grant OSTI 97-24412) for partial funding of the 500 MHz NMR spectrometer.

Supporting Information Available: Structural data in CIF format. This material is available free of charge via the Internet at <http://pubs.acs.org>.

IC049581+

(34) Hahn, T. *International Tables for Crystallography*; Kluwer Academic Publishers: Dordrecht, The Netherlands, 1992.

(35) Sheldrick, G. M. *SADABS*, version 2.10; Bruker AXS Inc.: Madison, WI, 2003.